Uptake of unnatural trehalose analogs as a reporter into *Mycobacterium tuberculosis*

Keriann M. Backus, Helena Boshoff, Conor S. Barry, Omar Boutureira, Mitul K. Patel, Francois D'Hooge, Seung S. Lee, Laura E. Via, Kapil Tahlan, Clifton E. Barry III, Benjamin G. Davis

School of Chemistry, University of Southampton, Southampton UK SO17 1BJ. E-mail: S.S.Lee@soton.ac.uk

Please cite this paper as:

Nature Chemical Biology, 2011, *7,* 228–235

The publisher's version of this paper is available here:

http://dx.doi.org/ 10.1038/nchembio.539

Incorporation of unnatural trehalose analogs into *Mycobacterium tuberculosis*: fluorescent probes of mycobacterial infection

Keriann M. Backus[a,b], Helena Boshoff[b], Conor S. Barry[a], Omar Boutureira[a], Mitul K. Patel[a], Francois D'Hooge[a] , Seung S. Lee[a], Laura E. Via[b], Kapil Tahlan[b], Clifton E Barry III[b*], Benjamin G. Davis[a*]

[a] Department of Chemistry, University of Oxford, Chemistry Research Laboratory, 12 Mansfield Road, Oxford OX1 3TA, UK; Ben.Davis@chem.ox.ac.uk

[b] Tuberculosis Research Section, Laboratory of Clinical Infectious Diseases, National Institute of Allergy and Infectious Disease, 33 North Drive, Bethesda, Maryland 20892, USA; CBARRY@niaid.nih.gov

Abstract (152 words)

The diagnosis of tuberculosis (TB) currently relies upon insensitive and non-specific techniques such as X-ray exams and acid-fast microscopy; newer diagnostics would ideally co-opt specific bacterial processes to provide real-time readouts of disease burden, bacterial viability and response to chemotherapy. The trehalose mycolyltransesterase enzymes (antigens 85A, B, and C (Ag85)) serve as essential mediators of cell envelope function and biogenesis in *Mycobacterium tuberculosis* (*Mtb*). We show here that the Ag85 enzymes have exceptionally broad substrate specificity, allowing exogenously added synthetic carbohydrate probes structurally similar to trehalose (Tre) to be incorporated into *Mtb* growing *in vitro* and within macrophages. Even very large substituents, such as in the fluorescein-containing Tre probe (FITC-Tre) were incorporated by growing bacilli thereby producing fluorescent bacteria. The addition of FITC-Tre to *Mtb*-infected macrophages allowed selective, sensitive detection of *Mtb*

within infected mammalian macrophages. These studies suggest that analogs of Tre may prove useful as probes for other imaging modalities.

Introduction

TB is an infection that has plagued mankind for millennia. It remains a leading cause of death worldwide and was implicated in an estimated 1.6 million fatalities in 2005[1]. A substantial obstacle to the development of new diagnostics, drugs, and vaccines is the lack of TB-specific probes that can be used to rapidly assess infection and monitor response to treatment[2]. The cell envelope of *Mtb* poses a significant permeability barrier that contributes to the intrinsic difficulties in eradicating this disease since it effectively precludes entry of most substances (including potential drugs and probes) to the bacterial cytoplasm[3-6].

The non-mammalian, disaccharide sugar trehalose, Tre (**1** , Scheme 1) is synthesized by *Mtb* through three independent pathways and genetic knockouts of any of these three pathways results in either non-viable *Mtb* or organisms displaying growth defects[7-11]. Because of this essentiality, targeting the trehalose pathway may be an important approach to TB drug development. Trehalose is found in the outer portion of the mycobacterial cell envelope along with the glycolipids trehalose dimycolate (TDM, Scheme 1) and trehalose monomycolate (TMM, Scheme 1).[12,13] TMM and TDM are important glycolipids for *Mtb*, capable of inducing granuloma formation in the absence of infection[14-16]. Mycolic acids are long (C60-C90), cyclopropanated lipids found in the cell wall of *Mtb*, which are important for bacterial outer membrane structure, virulence and persistence within the host.[17] Tre is anchored into the mycobacterial cell wall as mono- (TMM) or di- (TDM) mycolates by the action of the extracellular proteins Ag85 A, B, and C. Although these proteins were long known to immunologists by virtue of their immunogenicity, their enzymatic activity was first described in 1982 as the active fraction of a cell free extract from *Mycobacterium smegmatis* that was capable of synthesizing TDM[18]. Ag85A, Ag85B and Ag85C are the most abundant secreted *Mtb* proteins

in vitro, accounting for as much as 41% of the total protein in culture supernatant[19]. Individual knockouts of the genes that code for single members of the Ag85 family have significant effects on total cellular mycolic acid content[20-22]; triple knockouts of the *ag85ABC* genes have not been reported in *Mtb*, presumably because they are not viable. Ag85 isoforms all catalyse the reversible transesterification reaction between two units of TMM, generating TDM and free Tre (Scheme 1); the reverse reaction also allows for direct esterification of Tre. Ag85 can also covalently introduce mycolates into arabinogalactan to form the base polymer of the cell wall[22,23].

<Scheme 1>

Ag85A, Ag85B, and Ag85C share high sequence and structural homology [24-26], characterized by an α,β-hydrolase fold and a hydrophobic fibronectin-binding domain. Their active sites are highly conserved, featuring a His, Asp/Glu, Ser catalytic triad, a hydrophobic tunnel for the lipids and two trehalose binding sites (Figure 1a). These characteristics suggest a transesterification mechanism analogous to that of serine hydrolases, in which the formation of a covalent Ser-mycolic acid enzyme intermediate is followed by attack from the 6-hydroxyl of Tre[24].

<Figure 1>

Structural analysis (Figure 1b) of Tre bound to Ag85B suggested positions (C-4' and C-2) on Tre that were directed outward towards solvent and that might tolerate substitutions and yet retain activity as substrates for Ag85. Although trehalose itself has been demonstrated to be a substrate of Ag85[18,27,28] and its uptake and utilization by *M. smegmatis* has been observed,[10,29] Tre uptake into whole-cells of *Mtb* has not been investigated in detail[30,31] and corresponding

activities of Tre analogs have not been explored. We show here that not only are Ag85A, Ag85B and Ag85C sufficiently promiscuous to process a variety of trehalose analogs with good efficiency but that trehalose and Tre-probe analogs are also efficiently anchored to *Mtb*. We have exploited this substrate tolerance by designing fluorescent trehalose probes that are processed by Ag85 and that allow fluorescent labeling of *Mtb* in a selective manner. Our findings arm tuberculosis biologists with the first fluorescent small-molecule probe to label *Mtb* not only in culture but also in infected macrophages.

RESULTS

Exogenous Trehalose is incorporated into TMM and TDM by Whole cells of *Mtb*

We first sought to conclusively demonstrate that trehalose is taken up by live cells of *Mtb in vitro*. Unlike its fast-growing relative *M. smegmatis* which has 28 sugar transporters, the genome of *Mtb* encodes only five sugar permeases, suggesting that extracellular trehalose might not be efficiently taken up by mycobacteria[29,32]. Extracellular incorporation of Tre into TMM or TDM, on the other hand, would not require transport across the cell envelope. Using comparative radioprobes ^{14}C-acetate, ^{14}C-glycerol, ^{14}C-glucose and ^{14}C-trehalose we measured uptake in pathogenic *Mtb* over 2 and 24h time periods (Figures 2a and S1)[33]. Tre uptake was significant and the strongest band labeled by ^{14}C-Tre co-migrated with a band labeled by ^{14}C-acetate and co-migrated with cold TMM. ^{14}C-Tre also labeled a band that co-migrated with TDM, although not labeled to the same extent as TMM. To confirm that these bands were TMM and TDM we also labeled cells following treatment with isoniazid (INH), which inhibits mycolic acid biosynthesis and therefore blocks production of both TMM and TDM. As shown in Figure 2c (lanes 3 and 4)

INH effectively blocks biosynthesis of these two bands. Together these results demonstrated that Tre is taken up by the bacteria and incorporated into TDM and TMM by *Mtb in vitro*.

Mtb is thought to infect the alveolar macrophages that line the lung epithelium; macrophage uptake therefore represents an additional permeability hurdle that separates any potential probe from *Mtb*.[34] We therefore labeled *Mtb*-infected J774 cells (a murine macrophage-like cell line) and separately analyzed the macrophage supernatant, crude lysate and insoluble fractions (Figure 2b) of both infected and uninfected cells. Not only did ^{14}C-Tre successfully penetrate and internalize into murine macrophages, it was also subsequently taken up by *Mtb* growing within these cells, thereby validating the potential of Tre probes *in vivo*.

<Figure 2 >

Design and Synthesis of a Tre-analog Library

To fully explore the potential of Tre analogs as possible selective probes of *Mtb*, we designed and synthesized (see SI for details) a panel of compounds (Scheme 2) that would allow us to evaluate the substrate tolerance of Ag85 isoforms. This library of Tre analogs featured systematic modifications at each position to explore the enzyme active site in detail. Such trehalose derivatives present unique synthetic challenges: creating the link between the two glucose units requires that two difficult[35] stereocenters be established simultaneously and the symmetry of the Tre scaffold itself necessitates potentially complex asymmetric modifications. Elegant intramolecular, aglycone-tethered glycosylation strategies[36] have allowed access to some C-2 modifications and stereocontrol, yielding the α,α(1,1)-anomeric configuration found in natural Tre, but are limited in their scope of diversification. Most previous modifications of the

Tre scaffold, including previously designed inhibitors of Ag85, have focused only on modifications at C-6 and C-4[28,37-42].

Our Tre-probe library was synthesized using complementary strategies for i) directly creating the 1,1-linkage in Tre (Scheme S1) and ii) precise Tre scaffold alteration (Scheme S1) allowing access to analogs **2-22** bearing alterations in both the functional groups and in the stereochemical configurations found at all positions C-1, 2, 3, 4 and 6 in Tre. Functional groups were chosen for incorporation that might provide later use in the design of imaging probes such as fluorine (2-F, 3-F, 4-F, 6-F derivatives) for potential use in ^{18}F-PET and amines for late-stage attachment of chromophores, radiolabels and fluorophores.

1,1-Linkage formation was accomplished in three ways: a) ketoside formation[43-49] b) dehydrative glycosylation[50] and c) chemoenzymatically[9,51,52]. Full characterization of the synthesized probes included unambiguous assignment of stereochemistry using NMR (NOE and H-1 coupling constants). Methyl ketosides and exo-glycals proved to be excellent reagents for α,α-selective synthesis of asymmetric trehalose from a wide range of modified coupling partners, including derivatives of glucose, 2-deoxy-2-fluoro-glucose, 3-deoxy-3-fluoro-glucose, and 2-*N*-carbobenzyloxy-amino-glucose, yielding Tre-analogs **2-7** in good overall yields (30-90%) after deprotection (see SI). Symmetric dideoxy **10**, diiodo **12** and difluoro **13,14** trehalose analogs were accessed through dehydrative dimerization reactions.[50] 2-deoxy-2-fluoro-trehalose **22** was synthesized using a multi-step enzymatic route. Finally, Tre-scaffold modifications employed regioselective protecting group manipulation[41,42,53-55] to allow selective asymmetric access and replacement of hydroxyl groups at positions 4 and 6 (see SI for full details).

<Scheme 2>

Together these synthetic routes allowed ready access to Tre analogs **2-22** containing modifications such as 1-methyl **2-9**, 2-fluoro **3,5,13,14,22**, 2-iodo **12**, 2-deoxy **10,11** 3-fluoro **6**, 4-fluoro **21**, 6-fluoro **20**, 6-bromo **19**, 6-phosphate **15-17**, 6-azido **18** and even stereoisomers **4,5,11** and allowed access to intermediates such as 2-amino-Tre **7** onto which imaging labels fluorescein (in **9**), fluorobenzyl (in **8**) and even quantum dots (in Tre-QD, see SI) could be coupled.

A Novel Assay of Trehalose Processing

The substrate specificity and a full kinetic analysis of the Ag85 enzymes has not previously been fully attempted, presumably because of the difficult nature of the radiochemical assay using natural substrates. Heterogeneity in the mycolic fatty acid chain length (C30-C90), as well as low solubility of both substrates and products in aqueous media has complicated prior assays. The widely employed ^{14}C-Tre radioassay[56] monitors ^{14}C-Tre radiolabel incorporation into TDM and TMM yielding, at best, approximate $k_{cat(app)}$ values; such assays have suggested that Ag85B has a lower (~20%) activity than Ag85A and Ag85C[56].

<Table 1>

<Scheme 3>

Mass spectrometric analysis[57,58] provided a rapid means to screen Tre analogs **1-24** as substrates of all Ag85 isoforms (Table 1). Ag85A, Ag85B and Ag85C were prepared and purified as previously described[56,59,60] (see SI Figures S2-S8). We designed an assay[58] based on the use of precise, homogeneous mono and dihexanoyl Tre substrates, which proved to be water soluble and readily turned over by Ag85 allowing the development of a broad Ag85 substrate screen (Scheme 3). A calibrated green-amber-red (GAR)[57,61] screen for catalysis of transfer of

the acyl chain from natural Tre to unnatural Tre-analog (Tre*), using these pure synthetic substrates allowed determination of relative reactivity ratios Tre*:Tre (Table 1). Importantly, this screen revealed a strong selectivity for Tre-like disaccharides over monosaccharides such as D-glucose (**23**) but a striking plasticity for all tested Tre analogs. Modifications on every position of the sugar scaffold were tolerated including even C-1 methyl groups at the crowded anomeric linkages in **2-9;** positive charges, such as in the 2-amino-trehalose **7** and even stereochemically 'incorrect' 2,2'-di-fluoro-αβ-manno-trehalose **14**. Even a previously reported inhibitor[56], 6-azido-Tre **18** and putative tetrahedral transition state analogs, such as trehalose-6-phosphate **16**, were also processed.

Prior reports of **18** as an inhibitor (albeit a weak one with a reported MIC against a related mycobacterial species of 200 μg/mL)[56] prompted us to examine the possibility that these analogs also induced growth inhibition; minimum inhibitory concentration (MIC) analysis was therefore carried out on key representative compounds (Table 1). Amongst these only 2,2'-dideoxy-lyxo-Tre **11**, which was not a substrate for any of the three Ag85 isoforms, showed an inhibitory effect (MIC 100 μg/mL). C-6 modified compounds that were processed well by Ag85 inhibited growth only at high concentrations (MIC 100-200 μg/mL). Notably, no growth inhibition with FITC-Tre was noted either *in vitro* or in infected macrophages (see SI Figure S9).

FITC-Tre Specifically Labels *Mtb In Vitro*

Next we explored the uptake of fluorescent probes in growing cells of *Mtb* (Figure 3). The pathogenic *Mtb* strain H37Rv was grown for 24 hours in the presence of FITC-Tre and then washed to remove unbound dye. A significant increase in fluorescence over time was observed

in bacteria exposed to FITC-Tre, relative to the autofluorescence of the control bacteria and relative to heat-killed *Mtb* that had been treated with FITC-Tre (Figure 3a, b). Heat-killed Mtb form large aggregates that are particularly difficult to wash adequately, perhaps contributing to the relatively high background observed in these organisms. To demonstrate that incorporation was specific we also monitored incorporation of FITC-Glucose into live cells of *Mtb* and found significantly less incorporation of label into cells (Figure 3b), consistent with the poor efficiency of glucose as a substrate for the Ag85 enzymes (and the unlikely uptake of this probe into the cell by glucose-specific transporters). To demonstrate that this incorporation was dependent upon Ag85 we obtained a mutant in Ag85C that has been previously reported to have 40% less mycolic acid incorporation into the mycobacterial cell wall[22]. This mutant incorporated approximately 30% less FITC-Tre than did wild type (Figure 3a), supporting our proposed mechanism of anchoring of FITC Tre through Ag85 mediated incorporation of mycolic acids. To unambiguously establish that FITC-Tre was localizing to cells by virtue of being esterified with mycolic acids we simultaneously labeled cells with both FITC-Tre and ^{14}C-acetate and isolated individual fluorescent spots by preparative TLC (Figure 3c). We did not make any attempt to characterize the other less polar spots of low abundance that also apparently incorporated FITC-Tre although these might reasonably be supposed to be other Tre-containing glycolipids found within the mycobacterial cell wall.[16] Saponification of these spots followed by methylation and TLC revealed that the strongly fluorescent spots carrying FITC-Tre were associated with lipids co-migrating with the characteristic triplet pattern of the three classes of mycolic acids (alpha, methoxy and keto) (Figure 3e). Finally to establish specificity of labeling we also exposed three other organisms commonly found in the human lung to FITC-Tre; *Staphylococcus aureus*,

Haemophilus influenzae and *Pseudomonas aeruginosa*. None of these organisms were found to exhibit appreciable labeling with FITC-Tre (Figure 3b).

<Figure 3>

The value of FITC-Tre as a probe was demonstrated in its revelation of clear patterns of differential accumulation within live *Mtb* (Figure 4). For example, confocal fluorescence microscopy of H37Rv-*Mtb* expressing a red fluorescent protein (RFP, here mCherry carried by a PMV261 plasmid) revealed higher levels of green fluorescence from FITC-Tre incorporation at outer membranes and, in particular, at the bacterial poles, and less in mid sections (where the RFP localizes, Figure 4b-d). This specific localization was confirmed by microscopic sections along the Z-axis (Z-stacks, Figure 4e) and by statistical analysis of mean fluorescence ($p < 0.0001$, Figure 4f). These observations are not only consistent with the mode of action proposed for these Tre analogs but also suggest higher Ag85 activities at poles that appear consistent with a polar growth model.

<Figure 4>

FITC-Tre Specifically Labels *Mtb In Vitro* and Inside Mammalian Macrophages

We next tested the ability of these probes to selectively label *Mtb* in mammalian cells during infection. Treatment of *Mtb*-infected macrophages with FITC-Tre (Figure 5) demonstrated that the probe was internalized into macrophages with subsequent labeling of the bacteria (Figure 5a-c). The specificity of the label for *Mtb* was demonstrated by colocalization of staining with an *Mtb*-specific antibody (ab905, see SI), use of an alternative labeling strategy, and failure to observe labeling with FITC-Glucose (see SI Figures S10-S12). Labeling of the intra-macrophage

bacteria was also effectively abolished by competing administration of high concentrations (10-100mM) of trehalose (SI Figures S13,14).

<Figure 5>

In contrast to the fairly uniform labeling of bacilli observed in vitro, bacterial labeling *in vivo* was not uniform, either between cells or within a cell. We observed the same polar localization of label in *in vivo* grown cells seen in the *in vitro* cells, however some bacterial cells appeared to incorporate no label at all. By incorporating a constitutively expressed red fluorescent protein (RFP) in the infecting bacilli (either integratively transformed *M. bovis* BCG expressing the ds-red-1 gene,[62] or the H37Rv-*Mtb* mCherry variant (see above) for comparison) we observed that even mycobacterial cells within a single macrophage displayed very different labeling intensities (Figure 5d-f, g, k). We speculated that this differential FITC-Tre labeling might be relevant to the growth status of a particular bacterium within the cell reflective of the maturation status of the endosomal compartment within which they were located. TDM has been shown to inhibit fusion between vesicles[63] and is potentially responsible for the inhibition of phagosomal acidification by *Mtb*[64,65]. To test this hypothesis, murine bone marrow macrophages were infected with RFP-expressing H37Rv and treated with FITC-Tre, with or without activation by interferon-γ (IFN-γ). Colocalization studies were undertaken between the H37Rv and markers discriminating between endosomes, phagosomes and lysosomes, including the early endosome associated antigen (EEA-1), Rab5[66], Rab14[67], Pro-cathepsin D[68,69], and the lysosomal associated membrane protein (LAMP-1[70]). Colocalization was then assessed by confocal microscopy between these markers and the entire bacterial population as well as the highly FITC-Tre labeled subpopulation. As expected, low colocalization was observed both under activated and unactivated conditions for EEA-1 (see SI Figure S15). Consistent with previous reports of

accumulation of Rab5 in the mycobacterial phagosome, we observed consistent co-localization of this marker with both total, and high FITC-Tre-labeled bacilli in unactivated macrophages.

Upon IFN-γ activation, however, Rab5 colocalization was found to be less for highly FITC-Tre-labeled *Mtb* than the bulk bacterial population (Figure 5k-n). Colocalization between Rab14 and FITC-Tre-labeled *Mtb* compared to the total population of bacteria was comparable for both unactivated and IFN-γ treated macrophages (SI Figure S16). In contrast, Pro-Cathepsin D, cleavage of which is a marker of phagosomal maturation and phago-lysosome fusion was increased in colocalization with FITC-Tre-positive *Mtb* relative to the whole population (SI Figure S17). LAMP1 was also found to colocalize to a lesser degree with highly FITC-Tre positive bacteria (Figure 5g-j) than the population average, particularly upon IFN-γ activation. Together these data are consistent with the hypothesis that *Mtb* that poorly incorporate FITC-Tre tend to be localized to Rab5-containing phagosomes that have more fully matured towards degradative lysosomes. The corollary is that those with high Ag85-activity that incorporate FITC-Tre well, and will therefore readily generate TDM, are associated with less-developed phagosomes, perhaps through TDM-associated inhibitory mechanisms.[64,65]

Discussion

Despite decades of investigation for both their immunologic and enzymatic activities, the Antigen 85 enzymes remain poorly understood. Little is known about the range of their substrates and the reason for their apparent functional redundancy in *Mtb*. The uptake of ^{14}C-trehalose into *Mtb in vitro* as well as into infected macrophages suggested that Tre analogues may be useful in designing novel probes of TB pathogenesis. Using a novel Ag85 substrate assay

we have found that Ag85A,B and C will tolerate surprisingly extensive modifications on the trehalose scaffold, processing well many disaccharides (but not monosaccharides).

The discovery of the breadth of substrates processed by Ag85 isoforms could have important implications for the biological roles of these enzymes. The enzyme-specific differences in substrate tolerance observed imply an unappreciated subtlety in the active site architecture of these enzymes. Numerous glycolipids within *Mtb* contain a trehalose core, including, TDM, TMM, pentaacyl trehalose (PAT), triacyl trehalose (TAT) and sulfolipid-1 (Sl-1); little is known about the final acylation steps of PAT, TAT, and SL-1 and the enzymes of the Ag85 complex have been postulated to be involved in the lipidation of these compounds[71-73]. The substrate plasticity, particularly at the C-2 position, may also have implications in the final acylation steps of sulfolipid-1, which are unknown, but have been postulated to potentially occur *via* antigen 85[71,74]. Glucose and arabinose, both of which have been proposed as native enzyme substrates, are processed, albeit poorly relative to trehalose dissacharides[22,23,75]. The ability to fluorescently label lipids attached to trehalose by the Ag85 proteins should be useful in identifying other pathways that may employ their transesterification activity and help clarify this poorly understood area of biochemistry.

Most excitingly, these assays have informed the design of a fluorescent probe that selectively labels *Mtb* in infected macrophages. Prior imaging work with *Mtb* in infected macrophages has utilized several strategies[76-78] but none allow for non-toxic imaging of bacteria *in vivo*. Bacteria can be labeled with Texas-Red through oxidation with sodium periodate prior to infection. However, these harsh labeling conditions are nonselective and would be expected to oxidize carbohydrates that may be structurally important as well as peripherally associated glycolipids that may be important for specific virulence attributes.[76,77] Fluorescently-labeled vancomycin[79]

has been elegantly used to track the cell division patterns of *M. smegmatis* and *M. bovis* BCG[78] but its toxicity towards *Mtb*,[80] may affect experimental results. Antibodies can be utilized to label *Mtb* upon fixation and for enzyme linked immunosorbant assays (ELISA)[81], but are not useful for live imaging. FITC-Tre shows no significant inhibition of *Mtb* growth, which suggests that it does not perturb natural bacterial functions thereby allowing imaging of healthy, viable bacteria. FITC-Tre is also selective for *Mtb* and readily penetrates macrophages. Unlike other possible probes its mode of action is based on the activity of an enzyme unique to this genus of organisms. Given the highly conserved nature of the Ag85 proteins[82-84], in mycobacteria (and the complete absence of Tre in mammalian biology) it is likely this probe would also label non-tuberculous mycobacteria as well as other members of the tuberculosis complex.

Our understanding of the macrophage infection process is incomplete[85], so the ability to follow viable *Mtb* during infection shown here, could prove extremely useful as a means to further understand the bacterial transit to the phagosome as well as other intracellular compartments. The colocalization studies between FITC-Tre-labeled *Mtb* and various markers of phagosome maturation suggest that FITC-Tre may preferentially label those bacteria that resist acidification and phagosome-lysosome fusion. An alternative hypothesis that we cannot rule out is that incorporation of FITC-Tre into the membrane of a subset of bacilli alters the course of development of their phagosome, as has been seen with *Brucella pertusis* prelabeled with FITC before infection[86]. Since in our use of FITC-Tre it is added after the infection has been established, and is in low concentration relative to TDM, we expect the influence of the FITC-Tre-DM to be slight. Other trehalose-tagged molecules, potentially labeled at different positions or different tags on the trehalose scaffold may also prove useful as additional *Mtb* probes. Future work with FITC-Tre and related compounds will hopefully shed more light on its *in vivo*

potential, as a possible diagnostic tool to label *Mtb* in an infected host. Perhaps more excitingly, the broad substrate tolerance of the Ag85 proteins suggests the possibility of probes based on such analogs for a diverse panel of imaging modalities.

Methods

Chemical synthesis

The synthesis of all reported compounds is described in the Supplementary Methods.

Mass Spectrometry

Full details are described in the Supplementary Methods. Briefly, a 96-well plate was set up with each well containing TDH **60** and one of the screen compounds in 1mM TEA buffer (pH = 7.2) at 37 ˚C. To each well was added by automated injection (with mixing), 20 µL of either Ag85A/B/C or buffer alone to give final concentrations of 500 µM of each substrate and 2 µM of Ag85. The samples were incubated at 37 °C for 2h 40 min before injection of a 10 µL aliquot directly into the mass spectrometer. The resulting mass spectra were measured in ESI-continuum mode (150-1000 Da), corrected for baseline subtraction and smoothed. The peak intensities for mono-hexanoylated product and remaining substrate **26** were measured and the product/substrate ratio calculated for each well.

^{14}C-Trehalose uptake into infected macrophages

Murine J774 macrophage cells were grown to confluence in Dulbecco's MEM containing 10% fetal bovine serum, 1 mmol/L L-glutamine, and 1% pyruvate (DMEM) in two 75 mL tissue culture flasks. The medium was exchanged and one flask of cells was infected with an MOI of 10 *Mtb*/macrophage of H37Rv bacteria. After 3 h, cells were washed with DMEM. Following 24 h incubation, the medium was exchanged and ^{14}C-Trehalose (10 µCi) was added to both infected and uninfected cultures. Cells were incubated with ^{14}C-trehalose for a further 24 h. Media was removed and the supernatant clarified by centrifugation. Macrophages were gently washed with DMEM and lysed with PBS containing SDS 0.1% (10 mL). Cells were further washed with PBS buffer (2 × 5 mL) and lysate was

collected in falcon tubes and vortexed (1 min). The lysate was centrifuged at 3600 rpm for 20 min and supernatant was poured off and collected for scintillation counting. The pelleted *Mtb*, as well as controls were treated with four wash cycles of pelleting and resuspension (4 × 800 µL PBS with 0.1% Tween 80). The pellet was resuspended in a minimal amount of PBS (200 µL) and added to scintillation fluid.

^{14}C- and FITC-Tre lipid extractions

Lipid extractions from bacteria treated with ^{14}C-trehalose and ^{14}C-acetate and were conducted based on adaptations of radiolabelling from previous reports[87] and analyzed by radiographic TLC. ^{14}C-trehalose (10 µCi/tube) or ^{14}C-acetate (30 µCi/tube) or dual ^{14}C-acetate (30 µCi/tube) and FITC-trehalose (to final concentration of 100 µM) were added to 15 mL H37Rv OD_{650} of 0.8. Cells were harvested and extracted into 2 mL (2:1 chloroform:methanol). The organic layer was removed, concentrated and the residue was resuspended in 200 µL (80:20 chloroform:methanol) and 50 µL was spotted onto silica TLC plates, which were developed for 1 hour (75:25:4 chloroform:methanol:water). Plates were scanned for fluorescence and exposed to a phosphor storage plate, which was scanned for radioactivity. See Supplementary Methods for isoniazid inhibition of mycolate synthesis and mycolate saponification.

FITC-Tre and FITC-Glc uptake into *Mtb*

To CDC1551 *Mtb* or the Ag85C mutant of CDC1551(TBVTRM) in Middlebrook 7H9 media (10 mL) at an OD_{650} of 0.44 was added FITC-Tre **9** in ethanol to a final concentration of 100µM. Heat-killed (80 ˚C, 60 min) bacteria (2 × 0.5 mL) at an OD_{650} of 0.6 were used as control. *Mtb* were incubated at 37 °C with shaking. After 8 hours, the culture (4 × 400 µL) was harvested by centrifugation (1 min, 12000 rpm) and washed (3 x 1 mL 7H9 media) and resuspended (200 µL 7H9). Fluorescence measurements were conducted in 96-well format in appropriate plates (Nunc, Cat No 137103 (Roskilde, Denmark)). The background of the culture was obtained from cells treated in an identical fashion in the absence of FITC-Tre. Experiments were conducted in quadruplicate. Uptake was normalized for increase in OD_{650}. FITC-Glc **28** uptake (100µM) into CDC1551 and FITC-Tre **9** uptake into *H. influenza*e, *P. aeruginosa* and *S. aureus* was conducted in an analogous manner.

Visualization of FITC-Tre uptake into infected macrophages

In vitro: H37Rv-*Mtb* expressing RFP were grown in 7H9 medium to an OD = 0.25 at which point FITC-Tre **9** in ethanol was added to a final concentration of 200 μM and the culture was incubated with shaking for 24 h. The culture was then harvested and washed (3 × 1 mL PBS) by centrifugation and fixed in 5% formalin (1:1 in PBS). The culture was pelleted and resuspended in PBS (200 μL) and mounted in suitable medium (Prolong GOLD, Invitrogen).

In vivo: Bone Marrow macrophages (BMMs) were obtained as reported previously[88]. J774 Macrophages and BMMs were grown to confluence in supplemented DMEM on sterile coverslips. Cells treated with IFN-γ were exposed to 5 ng/mL mouse IFN- γ (Thermo RM200120) 18 hours prior to infection. BMMs and J774s were infected with H37Rv *Mtb* (2-3 bacteria/macrophage). After 4 h of infection, macrophages were washed to remove free bacteria and FITC-Tre **9** was added in ethanol to a 200 μM final concentration. IFN-γ was replenished after washing. Red fluorescent protein (RFP) expressing BCG and H37Rv were infected using an identical procedure. Cells were fixed at different timepoints (24 h or 40 h) in 5% formalin (1:1 in PBS) and coverslips were permeabalized, blocked and labeled with primary and secondary antibodies (see SI for full details), following standard immunocytochemical methods. Cells treated with just FITC-Tre **9** were mounted in the same manner, in the absence of antibody. For cells labeled with DAPI, a 0.1 mg/mL stock solution of DAPI was made up in DMF and cells were incubated with 1μg/mL DAPI solution for 5 minutes immediately prior to mounting.

Microscopy

Images of stained cells were obtained by confocal microscopy (Leica SP5 equipped with AOBS and a white light laser, Leica Microsystems, Exton, PA) using a 63× oil immersion objective NA 1.4. Images were gathered sequentially and stacked when DAPI was used to label cell so as to minimize cross-talk between channels. Essential sequential Z sections of stained cells were also recorded for generation of stacked images through cell. A 3-D volume was constructed from sequential Z sections of cells assembled into a 3D volume in Imaris software (version 7.0.0, Bitplane AG, Zurich, Switzerland). All collected images for analyses were deconvoluted by Huygens Essential software (Version 3.4, Scientific Volume Imaging BV, Hilversum, The Netherlands). Percentage colocalization was calculated using the colocalization function in Imaris. ROIs for the poles and mid-sections were

quantitated using the 'marching cubes' tool in Imaris to manually generate surfaces from which statistics were calculated for the regions of interest.

Further experimental details can be found in the Supplementary Methods.

Author Contributions K.M.B., H.B., C.S.B., L.E.V. C.E.B. and B.G.D. designed experiments. K.M.B., O.B., M.P., F.D'H. and S.S.L synthesized compounds. K.M.B., K.T. and H.B. performed uptake experiments. C.S.B. and K.M.B. performed substrate screens. K.M.B., H.B., C.S.B., C.E.B. and B.G.D. analyzed results. K.M.B., C.E.B. and B.G.D wrote the paper.

Acknowledgments

We thank Dr Tim Claridge, Dr Barbara Odell, Miss Tina Jackson for assistance with NMR spectra and Mr. Colin Sparrow, Dr James McCullagh, Mr. Robin Procter for their assistance with mass spectrometry. Dr. Owen Schwartz, Dr Lily Koo, Dr Matthew Gastinger, Dr Steven Becker, and Dr Juraj Kabat provided tremendous assistance on all imaging of *Mtb*. We thank the Colorado State "TB Vaccine Testing and Research Materials" Contract and Prof. Gideon Davies for providing Ag85 and OtsA plasmids, respectively. We thank Dr Taegown Oh for H37Rv carrying the mCherry-PMV261 plasmid. Alan Sher for *M. bovis* BCG expressing ds-red-1 and Dr. This study was supported (in part) by the Intramural Research Program of the National Institutes of Health, National Institute of Allergy and Infectious Disease (C.E.B.), by the Rhodes Trust (K.M.B.), a Marie Curie Intra European Fellowship (O.B.), the EPSRC (Platform Grant to B.G.D.) and the Bill and Melinda Gates Foundation through the TB Drug Accelerator Program (C.E.B, B.G.D.).

References

1. WHO. Global Tuberculosis Control Report 2008. (2008).
2. Young, D.B. Confronting the scientific obstacles to global control of tuberculosis. *J. Clin. Invest.* **118**, 1255-1265 (2008).
3. Brennan, P.J. & Nikaido, H. The envelope of mycobacteria. *Annu. Rev. Biochem.* **64**, 29-63 (1995).
4. Daffe, M. & Etienne, G. The capsule of Mycobacterium tuberculosis and its implications for pathogenicity. *Tuber. Lung. Dis.* **79**, 153-69 (1999).
5. Brennan, P.J. Structure, function, and biogenesis of the cell wall of Mycobacterium tuberculosis. *Tuberculosis* **83**, 91-97 (2003).
6. Alderwick, L.J., Birch, H.L., Mishra, A.K., Eggeling, L. & Besra, G.S. Structure, function and biosynthesis of the Mycobacterium tuberculosis cell wall:arabinogalactan and lipoarabinomannan assembly with a view to discovering new drug targets. *Biochem. Soc. Trans.* **35**, 1325-8 (2007).
7. De Smet, K.A., Weston, A., Brown, I.N., Young, D.B. & Robertson, B.D. Three pathways for trehalose biosynthesis in mycobacteria. *Microbiology* **146**, 199-208 (2000).
8. Murphy, H.N. et al. The OtsAB pathway is essential for trehalose biosynthesis in Mycobacterium tuberculosis. *J. Biol. Chem.* **280**, 14524-9 (2005).
9. Gibson, R.P., Turkenburg, J.P., Charnock, S.J., Lloyd, R. & Davies, G.J. Insights into Trehalose Synthesis Provided by the Structure of the Retaining Glucosyltransferase OtsA. *Chem. Biol.* **9**, 1337-1346 (2002).
10. Woodruff, P.J. et al. Trehalose is required for growth of Mycobacterium smegmatis. *J. Biol. Chem.* **279**, 28835-43 (2004).

11. Barry, C.E., Crick, D.C. & McNeil, M.R. Targeting the formation of the cell wall core of M. tuberculosis. *Infect. Disord. Drug Targets* **7**, 182-202 (2007).

12. Ortalo-Magne, A. et al. Identification of the surface-exposed lipids on the cell envelopes of Mycobacterium tuberculosis and other mycobacterial species. *J. Bacteriol.* **178**, 456-461 (1996).

13. Hoffmann, C., Leis, A., Niederweis, M., Plitzko, J.M. & Engelhard, H. Disclosure of the mycobacterial outer membrane: Cryo-electron tomography and vitreous sections reveal the lipid bilayer structure. *Proc. Natl Acad. Sci. USA* **105**, 3963-3967 (2008).

14. Puissegur, M.-P. et al. An in vitro dual model of mycobacterial granulomas to investigate the molecular interactions between mycobacteria and human host cells. *Cell. Microbiol.* **6**, 423-433 (2004).

15. Yamagami, H. et al. Trehalose 6,6'-dimycolate (cord factor) of Mycobacterium tuberculosis induces foreign-body- and hypersensitivity-type granulomas in mice. *Infect. Immun.* **69**, 810-5 (2001).

16. Kastrinsky, D., Mcbride, N., Backus, K.M., Leblanc, J. & Barry, C.E.I. The Chemical Biology of the Complex Lipid-Containing Virulence Factors of the Mycobacterial Cell Envelope. in *Comprehensive Natural Products Chemistry* (ed. Townsend, C.A.) 65-146 (Elsevier, Oxford, 2010).

17. Barry, C.E. & Mdluli, K. Drug sensitivity and environmental adaptation of mycobacterial cell wall components. *Trends in Microbiology* **4**, 275-281 (1996).

18. Kilburn, J.J.O., Takayama, K.K. & Armstrong, E.E.L. Synthesis of trehalose dimycolate (cord factor) by a cell-free system of Mycobacterium smegmatis. *Biochem. Biophys. Res. Commun.* **108**, 132-9 (1982).

19. Fukui, Y., Hirai, T., Uchida, T. & Yoneda, M. Extracellular proteins of tubercle bacilli. IV. Alpha and beta antigens as major extracellular protein products and as cellular components of a strain (H37Rv) of Mycobacterium tuberculosis. *Biken J.* **8**, 189-99 (1965).

20. Harth, G., Horwitz, M.A., Tabatadze, D. & Zamecnik, P.C. Targeting the Mycobacterium tuberculosis 30/32-kDa mycolyl transferase complex as a therapeutic strategy against tuberculosis: Proof of principle by using antisense technology. *Proc. Natl Acad. Sci. USA* **99**, 15614-9 (2002).

21. Puech, V. et al. Evidence for a partial redundancy of the fibronectin-binding proteins for the transfer of mycoloyl residues onto the cell wall arabinogalactan termini of Mycobacterium tuberculosis. *Mol Microbiol* **44**, 1109-22 (2002).

22. Jackson, M. et al. Inactivation of the antigen 85C gene profoundly affects the mycolate content and alters the permeability of the Mycobacterium tuberculosis cell envelope. *Mol. Microbiol.* **31**, 1573-87 (1999).

23. Puech, V., Bayan, N., Salim, K., Leblon, G. & Daffe, M. Characterization of the in vivo acceptors of the mycoloyl residues transferred by the corynebacterial PS1 and the related mycobacterial antigens 85. *Mol. Microbiol.* **35**, 1026-41 (2000).

24. Ronning, D.R. et al. Crystal structure of the secreted form of antigen 85C reveals potential targets for mycobacterial drugs and vaccines. *Nat. Struct. Biol.* **7**, 141-6 (2000).

25. Anderson, D.H., Harth, G., Horwitz, M.A. & Eisenberg, D. An interfacial mechanism and a class of inhibitors inferred from two crystal structures of the Mycobacterium tuberculosis 30 kDa major secretory protein (Antigen 85B), a mycolyl transferase. *J. Mol. Biol.* **307**, 671-81 (2001).

26. Ronning, D.R., Vissa, V., Besra, G.S., Belisle, J.T. & Sacchettini, J.C. Mycobacterium tuberculosis antigen 85A and 85C structures confirm binding orientation and conserved substrate specificity. *J. Biol. Chem.* **279**, 36771-7 (2004).

27. Wang, J. et al. Synthesis of trehalose-based compounds and their inhibitory activities against Mycobacterium smegmatis. *Bioorg. Med. Chem.* **12**, 6397-413 (2004).

28. Ohta, M., Pan, Y.T., Laine, R.A. & Elbein, A.D. Trehalose-based oligosaccharides isolated from the cytoplasm of Mycobacterium smegmatis. Relation to trehalose-based oligosaccharides attached to lipid. *Eur. J. Biochem.* **269**, 3142-9 (2002).

29. Titgemeyer, F. et al. A Genomic View of Sugar Transport in Mycobacterium smegmatis and Mycobacterium tuberculosis. *J. Bacteriol.* **189**, 5903-5915 (2007).

30. Whilst this manuscript was submitted, early observations supporting the uptake of Tre by Mtb were published; see following reference.

31. Kalscheuer, R., Weinricka, B., Veeraraghavan, U., Besra, G.S. & Jacobs, W.R. Trehalose-recycling ABC transporter LpqY-SugA-SugB-SugC is essential for virulence of Mycobacterium tuberculosis. *Trehalose-recycling ABC transporter LpqY-SugA-SugB-SugC is essential for virulence of Mycobacterium tuberculosis* **doi: 10.1073/pnas.1014642108** (2010).

32. Deol, P. et al. Role of Mycobacterium tuberculosis Ser/Thr kinase PknF: implications in glucose transport and cell division. *J. Bacteriol.* **187**, 3415-20 (2005).

33. Stahl, C. et al. MspA provides the main hydrophilic pathway through the cell wall of Mycobacterium smegmatis. *Mol. Microbiol.* **57**, 1509-1509 (2005).

34. Tufariello, J.M., Chan, J. & Flynn, J.L. Latent tuberculosis: mechanisms of host and bacillus that contribute to persistent infection. *The Lancet Infectious Diseases* **3**, 578-590 (2003).

35. Demchenko, A.V. 1,2-cis O-Glycosylation: Methods, Strategies, Principles. *Curr. Org. Chem.* **7**, 35-79 (2003).

36. Pratt, M.R., Leigh, C.D. & Bertozzi, C.R. Formation of 1,1-alpha,alpha-glycosidic bonds by intramolecular aglycone delivery. A convergent synthesis of trehalose. *Org. Lett.* **5**, 3185-8 (2003).

37. Gobec, S. et al. Phosphonate inhibitors of antigen 85C, a crucial enzyme involved in the biosynthesis of the Mycobacterium tuberculosis cell wall. *Bioorg. Med. Chem. Lett.* **14**, 3559-62 (2004).

38. Gobec, S. et al. Design, synthesis, biochemical evaluation and antimycobacterial action of phosphonate inhibitors of antigen 85C, a crucial enzyme involved in biosynthesis of the mycobacterial cell wall. *Eur. J. Med.* **42**, 54-63 (2007).

39. Hui, Y. & Chang, C.W. Convenient divergent synthesis of a library of trehalosamine analogues. *Org. Lett.* **4**, 2245-8 (2002).

40. Jin, L.Q., Xue, Y.P., Zheng, Y.G. & Shen, Y.C. Production of trehalase inhibitor validoxylamine A using acid-catalyzed hydrolysis of validamycin A. *Catal. Commun.* **7**, 157-161 (2006).

41. Hadfield, A.F., Hough, L. & Richardson, A.C. The synthesis of 6-deoxy-6-fluoro-alpha,alpha-trehalose and related analogues. *Carbohydr. Res.* **63**, 51-60 (1978).

42. Hadfield, A.F., Hough, L. & Richardson, A.C. The syntheses of 4,6-dideoxy-4,6-difluoro- and 4-deoxy-4-fluoro-alpha,alpha-trehalose. *Carbohydr. Res.* **71**, 95-102 (1979).

43. Yamanoi, T., Inoue, R., Matsuda, S., Katsuraya, K. & Hamasaki, K. Synthesis of trehalose mimics by bismuth(III) triflate or bis(trifluoromethane)sulfonimide-catalyzed 1-C-methyl-D-hexopyranosylation. *Tetrahedron: Asymmetry* **17**, 2914-2918 (2006).

44. Namme, R., Hideyo, T.M. & Ikegami, T.S. Development of Ketoside-Type Analogues of Trehalose by Using Stereoselective O-Glycosidation of Ketose. *Eur. J. Org. Chem.* **2007**, 3758-3764 (2007).

45. Gomez, A.M., Pedregosa, A., Valverde, S. & Lopez, J.C. Stereoselective synthesis of substituted exo-glycals from 1-exo-methylene pyranoses. *Tetrahedron Lett.* **44**, 6111-6116 (2003).

46. Li, X., Ohtake, H., Takahashi, H. & Ikegami, S. A facile synthesis of 1'-C-alkyl-[alpha]-disaccharides from 1-C-alkyl-hexopyranoses and methyl 1-C-methyl-hexopyranosides. *Tetrahedron* **57**, 4297-4309 (2001).

47. Griffin, Frank K., Paterson, Duncan E., Murphy, Paul V. & Taylor, Richard J.K. A New Route to exo-Glycals Using the Ramberg-Bäcklund Rearrangement. *Eur. J. Org. Chem.* **2002**, 1305-1322 (2002).

48. Yang, W.B. et al. Stereochemistry in the synthesis and reaction of exo-glycals. *J. Org. Chem.* **67**, 3773-82 (2002).

49. Zhu, X., Jin, Y. & Wickham, J. Efficient Synthesis of Methylene exo-Glycals: Another Use of Glycosylthiomethyl Chlorides. *J. Org. Chem.* **72**, 2670-2673 (2007).

50. Rodriguez, M.A. et al. Synthesis of 2-Iodoglycals, Glycals, and 1,1'-Disaccharides from 2-Deoxy-2-iodopyranoses under Dehydrative Glycosylation Conditions. *J. Org. Chem.* **72**, 8998-9001 (2007).

51. Giaever, H.M., Styrvold, O.B., Kaasen, I. & Strom, A.R. Biochemical and genetic characterization of osmoregulatory trehalose synthesis in Escherichia coli. *J. Bacteriol.* **170**, 2841-9 (1988).

52. Gibson, R.P., Tarling, C.A., Roberts, S., Withers, S.G. & Davies, G.J. The donor subsite of trehalose-6-phosphate synthase: binary complexes with UDP-glucose and UDP-2-deoxy-2-fluoro-glucose at 2 A resolution. *J. Biol. Chem.* **279**, 1950-5 (2004).

53. Defaye, J., Driguez, H., Henrissat, B., Gelas, J. & Bar-Guilloux, E. Asymmetric acetalation of alpha,alpha-trehalose: Synthesis of alpha-galactopyranosyl alpha-glucopyranoside and 6-deoxy-6-fluoro-alpha-glucopyranosyl-alpha-glucopyranoside. *Carbohydr. Res.* **63**, 41-49 (1978).

54. Wang, M., Tu, P.-F., Xu, Z.-D., Yu, X.-L. & Yang, M. Design and Synthesis of Guanidinoglycosides Directed against the TAR RNA of HIV-1. *Helv. Chim. Acta* **86**, 2637-2644 (2003).

55. Lin, F.L., van Halbeek, H. & Bertozzi, C.R. Synthesis of mono- and dideoxygenated alpha,alpha-trehalose analogs. *Carbohydr. Res.* **342**, 2014-2030 (2007).

56. Belisle, J.T. et al. Role of the major antigen of Mycobacterium tuberculosis in cell wall biogenesis. *Science* **276**, 1420-2 (1997).

57. Yang, M. et al. Probing the breadth of macrolide glycosyltransferases: in vitro remodeling of a polyketide antibiotic creates active bacterial uptake and enhances potency. *J. Am. Chem. Soc.* **127**, 9336-7 (2005).

58. Barry, C., Backus, K.M., Barry, C.E., 3rd; & Davis, B.G. Precise ESI-MS kinetic analysis of the M. tuberculosis cell wall antigen-85 enzymes. *in preparation* (2009).

59. Boucau, J., Sanki, A.K., Voss, B.J., Sucheck, S.J. & Ronning, D.R. A coupled assay measuring Mycobacterium tuberculosis antigen 85C enzymatic activity. *Anal. Biochem.* **385**, 120-7 (2009).

60. Sanki, A.K., Boucau, J., Ronning, D.R. & Sucheck, S.J. Antigen 85C-mediated acyl-transfer between synthetic acyl donors and fragments of the arabinan. *Glycoconj. J.* (2008).

61. Flint, J. et al. Structural dissection and high-throughput screening of mannosylglycerate synthase. *Nat. Struct. Mol. Biol.* **12**, 608-14 (2005).

62. Abadie, V. et al. Neutrophils rapidly migrate via lymphatics after Mycobacterium bovis BCG intradermal vaccination and shuttle live bacilli to the draining lymph nodes. *Blood* **106**, 1843-1850 (2005).

63. Alvarez-Dominguez, C. & Stahl, P.D. Interferon-gamma Selectively Induces Rab5a Synthesis and Processing in Mononuclear Cells. *J. Biol. Chem.* **273**, 33901 (1998).

64. Alvarez-Dominguez, C. & Stahl, P.D. Increased expression of Rab5a correlates directly with accelerated maturation of Listeria monocytogenes phagosomes. *J. Biol. Chem.* **274**, 11459-62 (1999).

65. Barker, L.P., George, K.M., Falkow, S. & Small, P.L. Differential trafficking of live and dead Mycobacterium marinum organisms in macrophages. *Infect. Immun.* **65**, 1497-1504 (1997).

66. Fratti, R.A., Backer, J.M., Gruenberg, J., Corvera, S. & Deretic, V. Role of phosphatidylinositol 3-kinase and Rab5 effectors in phagosomal biogenesis and mycobacterial phagosome maturation arrest. *J. Cell Biol.* **154**, 631-644 (2001).

67. Duclos, S. et al. Rab5 regulates the kiss and run fusion between phagosomes and endosomes and the acquisition of phagosome leishmanicidal properties in RAW 264.7 macrophages. *J. Cell Sci.* **113**, 3531-3541 (2000).

68. Huynh, K.K. et al. LAMP proteins are required for fusion of lysosomes with phagosomes. *EMBO J.* **26**, 313-324 (2007).

69. Indrigo, J., Hunter, R.L., Jr. & Actor, J.K. Influence of trehalose 6,6'-dimycolate (TDM) during mycobacterial infection of bone marrow macrophages. *Microbiology* **148**, 1991-8 (2002).

70. Indrigo, J., Hunter, R.L., Jr. & Actor, J.K. Cord factor trehalose 6,6'-dimycolate (TDM) mediates trafficking events during mycobacterial infection of murine macrophages. *Microbiology* **149**, 2049-59 (2003).

71. Converse, S.E. et al. MmpL8 is required for sulfolipid-1 biosynthesis and Mycobacterium tuberculosis virulence. *Proc. Natl Acad. Sci. USA* **100**, 6121-6126 (2003).

72. Kumar, P. et al. PapA1 and PapA2 are acyltransferases essential for the biosynthesis of the Mycobacterium tuberculosis virulence factor Sulfolipid-1. *Proc. Natl Acad. Sci. USA* **104**, 11221-11226 (2007).

73. Hatzios, S.K. et al. PapA3 Is an Acyltransferase Required for Polyacyltrehalose Biosynthesis in Mycobacterium tuberculosis. *J. Biol. Chem.* **284**, 12745-12751 (2009).

74. Mougous, J.D. et al. Identification, function and structure of the mycobacterial sulfotransferase that initiates sulfolipid-1 biosynthesis. *Nat. Struct. Mol. Biol.* **11**, 721-729 (2004).

75. Matsunaga, I. et al. Mycolyltransferase-mediated Glycolipid Exchange in Mycobacteria. *J. Biol. Chem.* **283**, 28835-28841 (2008).

76. Beatty, W.L. et al. Trafficking and release of mycobacterial lipids from infected macrophages. *Traffic* **1**, 235-47 (2000).

77. Beatty, W.L. & Russell, D.G. Identification of Mycobacterial Surface Proteins Released into Subcellular Compartments of Infected Macrophages. *Infect. Immun.* **68**, 6997-7002 (2000).

78. Thanky, N.R., Young, D.B. & Robertson, B.D. Unusual features of the cell cycle in mycobacteria: polar-restricted growth and the snapping-model of cell division. *Tuberculosis* **87**, 231-6 (2007).

79. Daniel, R.A. & Errington, J. Control of Cell Morphogenesis in Bacteria: Two Distinct Ways to Make a Rod-Shaped Cell. *Cell* **113**, 767-776 (2003).

80. Provvedi, R., Boldrin, F., Falciani, F., Palu, G. & Manganelli, R. Global transcriptional response to vancomycin in Mycobacterium tuberculosis. *Microbiology-Sgm* **155**, 1093-1102 (2009).

81. Glatman-Freedman, A., Martin, J.M., Riska, P.F., Bloom, B.R. & Casadevall, A. Monoclonal antibodies to surface antigens of Mycobacterium tuberculosis and their use in a modified enzyme-linked immunosorbent spot assay for detection of mycobacteria. *J. Clin. Microbiol.* **34**, 2795-2802 (1996).

82. Cole, S.T. et al. Deciphering the biology of mycobacterium tuberculosis from the complete genome sequence. *Nature* **393**, 537-544 (1998).

83. Rinke de Wit, T.F. et al. The Mycobacterium leprae antigen 85 complex gene family: identification of the genes for the 85A, 85C, and related MPT51 proteins. *Infect. Immun.* **61**, 3642-7 (1993).

84. Ohara, N. et al. Analysis of the genes encoding the antigen 85 complex and MPT51 from Mycobacterium avium. *Infect. Immun.* **65**, 3680-5 (1997).

85. Schorey, J.S., Carroll, M.C. & Brown, E.J. A Macrophage Invasion Mechanism of Pathogenic Mycobacteria. *Science* **277**, 1091-1093 (1997).

86. Weingart, C.L. et al. Fluorescent labels influence phagocytosis of Bordetella pertussis by human neutrophils. *Infect. Immun.* **67**, 4264-4267 (1999).

87. Slayden, R.A. & Barry, C.E. Analysis of the Lipids of Mycobacterium tuberculosis. in *Mycobacterium tuberculosis Protocols*, Vol. 54 (eds. Parish, T. & Stoker, N.G.) 229-245 (Humana Press, 2001).

88. Celada, A., Gray, P.W., Rinderknecht, E. & Schreiber, R.D. Evidence for a gamma-interferon receptor that regulates macrophage tumoricidal activity. *J Experimental Med.* **160**, 55-74 (1984).

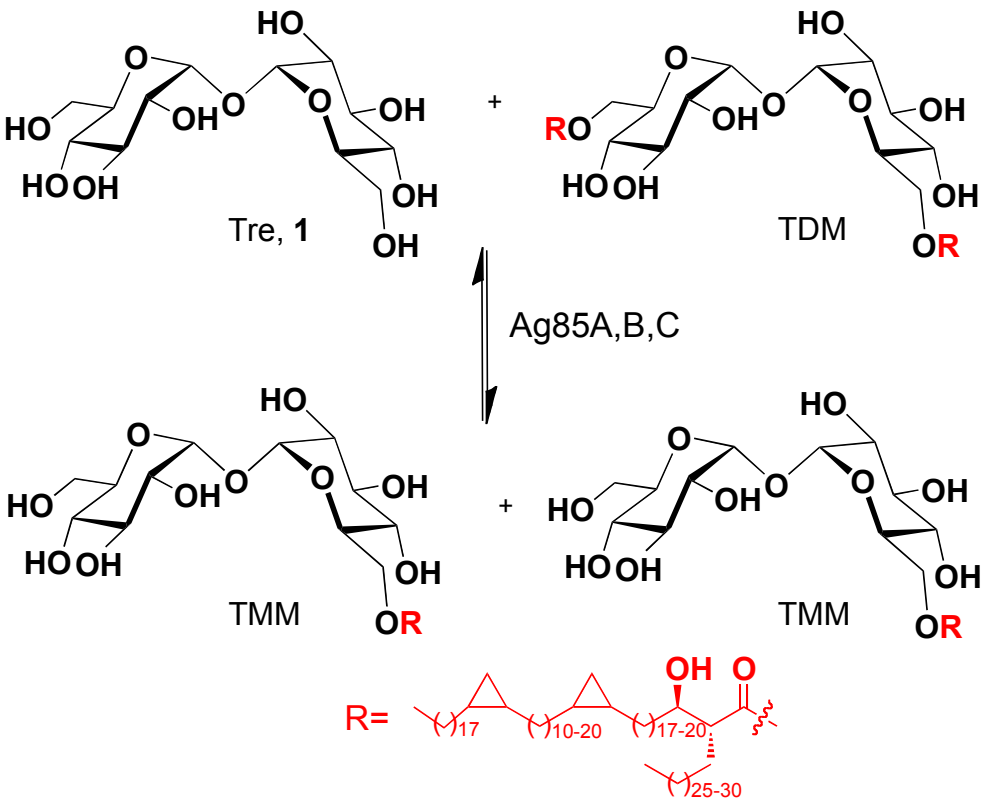

Scheme 1. Ag85A, Ag85B, and Ag85C catalyzed transesterification of trehalose **1**, trehalose dimycolate (TDM) and trehalose monomycolate (TMM).

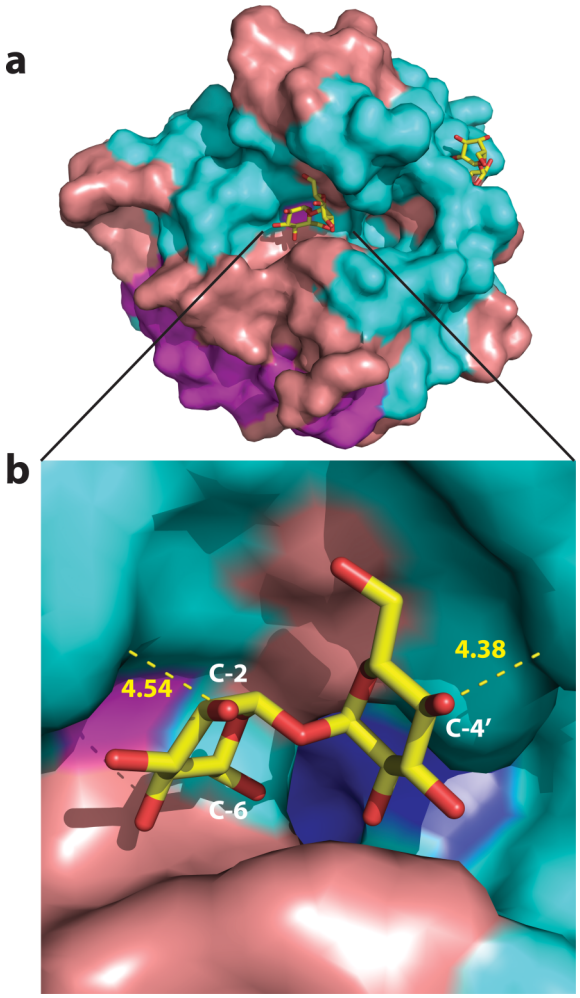

Figure 1. The x-ray crystal structure (PDB accession code 1F0P) of Ag85B suggests significant modification of trehalose substrates may be tolerated without altering binding contacts. (a) Ag85B in surface representation binds trehalose (stick model with carbon depicted as yellow and oxygen as red) in its active site as shown. (b) An expanded view of this active site region of Ag85B reveals that the C-2 and C-4′ hydroxyl groups of trehalose are directed out of the active site towards unobstructed regions. C-6 points into a hydrophobic tunnel (blue) that is thought to accommodate the long fatty acyl chains of the mycolic acids. Measurements of the distance from key trehalose atoms to the nearest residues in the protein are indicated in angstroms. Figure generated in Pymol.

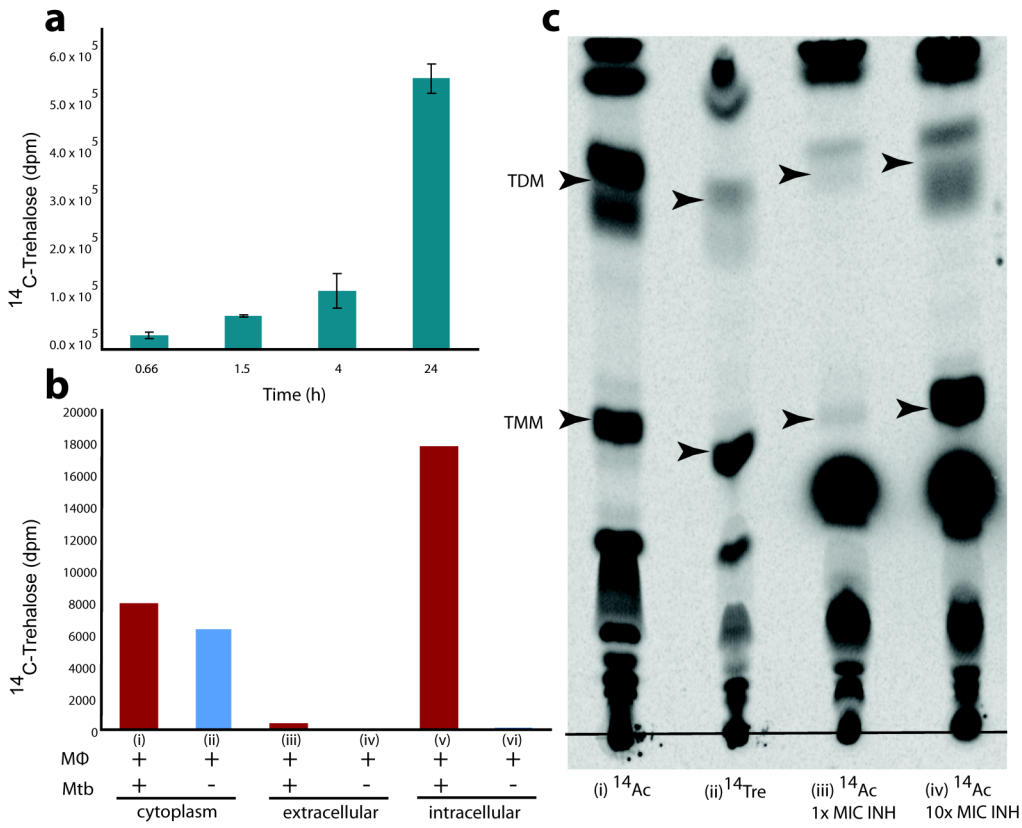

Figure 2. Exogenously added trehalose is incorporated into TMM and TDM *in vitro* and in macrophages infected with *Mtb*. (a) Incorporation of ^{14}C-trehalose into cell-associated counts in an *Mtb* culture over 24 h. (b) ^{14}C-trehalose was added either to *Mtb*-infected (i, iii, v), or to uninfected (ii, iv, vi) macrophages for 24 h. The supernatant was separated (and measured giving rise to 'extracellular' counts) and the macrophages were lysed prior to the separation of bacteria by centrifugation. The second supernatant resulting from this separation was measured for 'cytoplasm' counts and the pellet measured for 'intracellular'. Radioactive trehalose is found in the cytoplasm fraction of both infected and uninfected macrophages but is incorporated into mycobacterial cells in infected macrophages. (c) ^{14}C-trehalose is incorporated into TMM and TDM in *Mtb*. Arrowheads show the migration position of authentic samples of TMM and TDM. In the first lane the culture was labeled for 24 h with ^{14}C-acetate to label all fatty acids and then

extracted as described in the Methods. In the second lane the culture was labeled with ^{14}C-trehalose for 24 h and then extracted. In the third and fourth lanes the culture was treated with 10 × and 1× MIC concentrations of isoniazid (INH) to block the synthesis of mycolic acids and thereby inhibit formation of TMM and TDM. ^{14}C-Trehalose labels spots that co-migrate with TMM and TDM, the synthesis of which is blocked by INH.

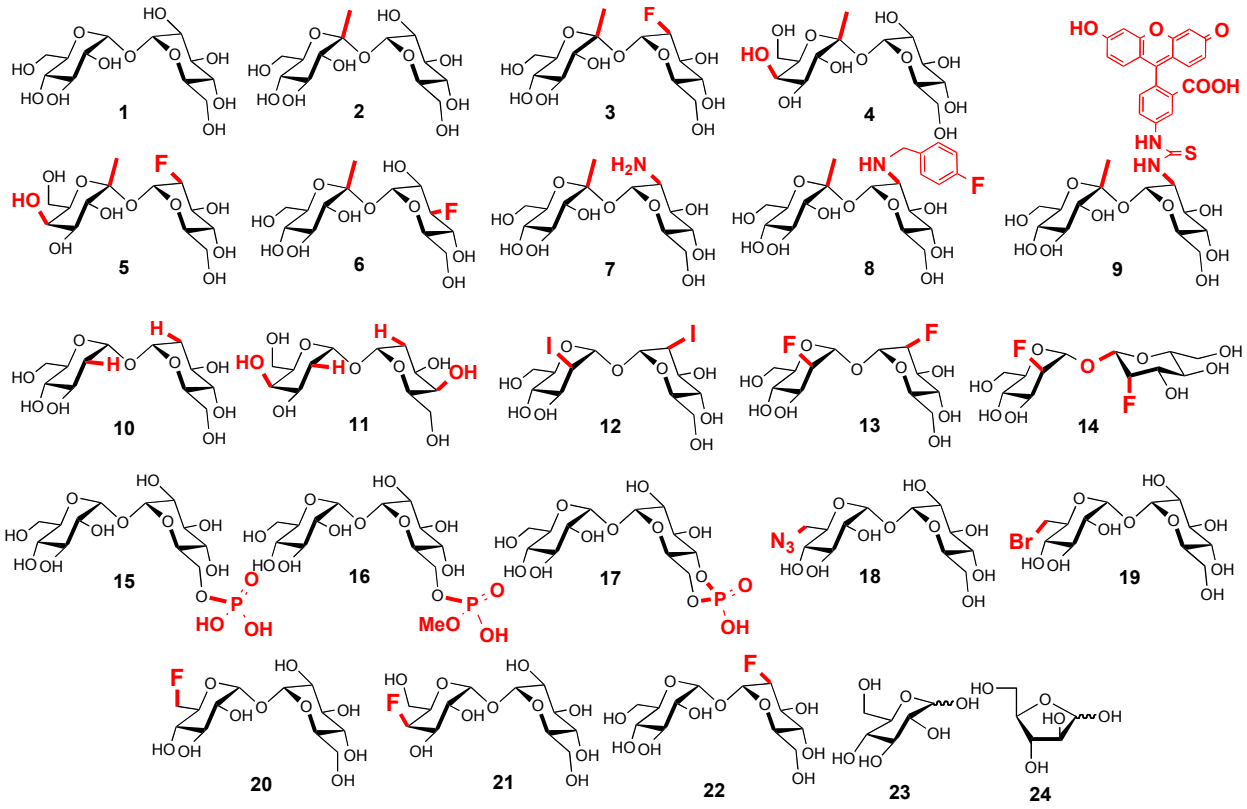

Scheme 2. Library of trehalose compounds and analogs. Numbered compounds correspond to those in the GAR screen (see Table 1). Key modifications in the trehalose analogs (**2**-**22**) are highlighted in red and bold. Synthesis and characterization of all compounds are described in the Supplementary Information.

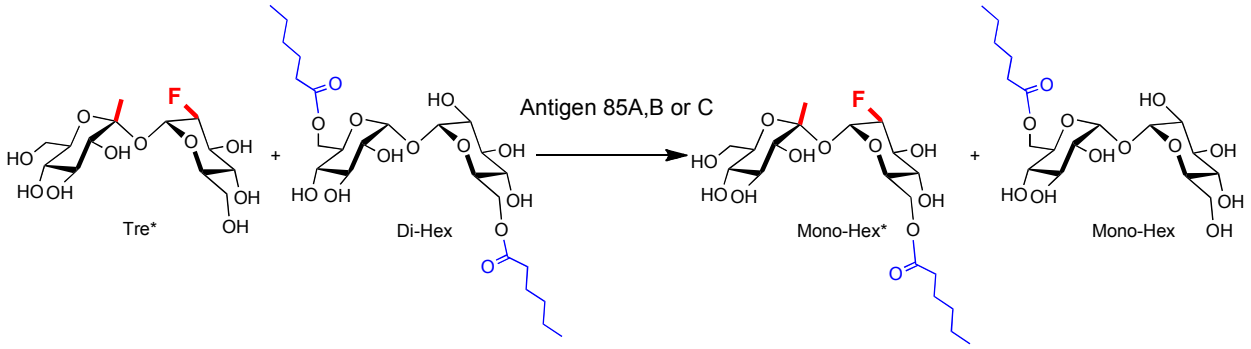

Scheme 3. Simplified Antigen 85 turnover assay. Tre* represents any trehalose analog (the chosen example here corresponds to compound **3** from the library but the assay uses essentially analogous reactions for all other substrates). Mass spectrometry is utilized to quantify the amount of acyl-transfer to the trehalose analog (forming, for example, Mono-Hex* from Tre*) by Antigen 85.

Table 1. Green-amber-red (GAR) screen of trehalose analogs. Compound numbers in Scheme 2 correspond to numbers in Table 1. The row detailing FITC-Tre compound **9** is shown in bold. Substrate response is expressed as percentage of the natural substrate response:>75% = Dark Green, 25-75% Light Green, 5-25% = Amber, <5% = Red. (Response = Peak height (mono-Hex*)/Peak height (Tre*)). Minimum inhibitory concentration (MIC). "†>200µg/mL" has some growth inhibition at 200 µg/mL. MIC_{50} = concentration causing 50% growth inhibition. ND = not determined.

Compound	**Ag85A**	**Ag85B**	**Ag85C**	**MIC**	**MIC_{50}**
1	100	100	100	>200 µg/mL	>200 µg/mL
2	32	13	111	>200 µg/mL	>200 µg/mL
3	73	1415	102	>200 µg/mL	>200 µg/mL
4	12	7	57	>200 µg/mL	>200 µg/mL
5	19	13	64	>200 µg/mL	>200 µg/mL
6	7	8	76	>200 µg/mL	>200 µg/mL
7	47	56	91	>200 µg/mL	>200 µg/mL
8	25	14	81	>200 µg/mL	>200 µg/mL
9	**31**	**38**	**44**	**>200 µg/mL**	**>200 µg/mL**
10	50	16	129	>200 µg/mL	>200 µg/mL
11	1	4	1	100 µg/mL	ND
12	148	54	166	>200 µg/mL	>200 µg/mL
13	66	24	98	>200 µg/mL	>200 µg/mL
14	38	35	82	>200 µg/mL	>200 µg/mL
15	6	4	28	>200 µg/mL	>200 µg/mL
16	37	24	113	†>200µg/mL	ND
17	18	17	94	>200µg/mL	>200µg/mL
18	37	13	49	†>200µg/mL	135 µg/mL
19	102	92	99	200µg/ml	134 µg/mL
20	149	412	91	200µg/ml	75 µg/mL
21	229	162	191	100µg/ml	50 µg/mL
22	115	156	274	>200 µg/mL	>200 µg/mL
23	18	19	45	>200 µg/mL	>200 µg/mL
24	6	28	8	>200 µg/mL	>200 µg/mL

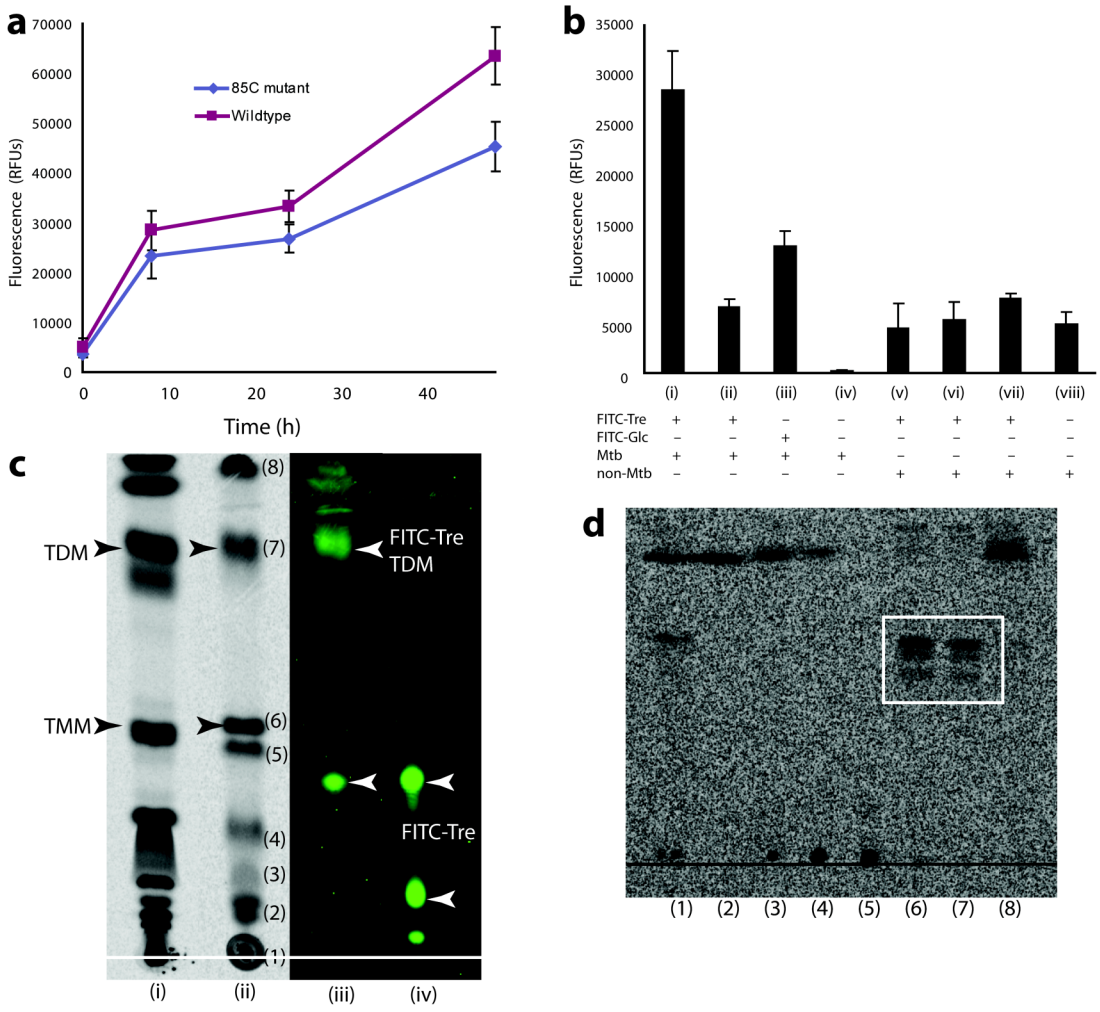

Figure 3. FITC-Tre is incorporated by *Mtb* into FITC-TDM through the action of the Ag85 enzymes. (a) Uptake of FITC-Tre into wildtype CDC 1551 (purple squares) or 85C mutant, known to have a 40% reduction in mycolic acid incorporation into the cell wall (blue diamonds). (b) Uptake of FITC-Tre or FITC-Glc into (i , iii, and iv), live *Mtb* (ii), heat killed *Mtb* (v), *Staphylococcus aureus* (vi), *Pseudomonas aeruginosa*, (vii) *Haemophilus influenza*, (viii) Mean autoflorescence of *H. influenza* as representative of autofluorescence of non-mycobacterial species. (c) FITC-Tre is incorporated into a dimycolate, as shown by dual labeling with FITCTre and ^{14}C-acetate. Lane (i) shows the radio-TLC from single labeling with ^{14}C-acetic acid. Lane

(ii) shows the radio-TLC that results from dual labeling using both ^{14}C-acetic acid and FITC-Tre. Lane (iii) shows the fluorescence intensity across the same lane as shown in (ii). Lane (iv) shows untreated FITC-Tre in the same TLC system. (d) The glycolipids extracted from these dual labeling experiments in co-migrate with TDM contain mycolic acids. (1)-(8) correspond to the individual spots labeled in lane (ii) of the radio-TLC shown in (c) that were excised, hydrolyzed to release fatty acids, methylated and run on a second TLC. The glycolipids in spots (6) and (7) contain lipids that co-migrate with authentic mycolic acids. These also display the characteristic banding pattern of the three major forms of these lipids.

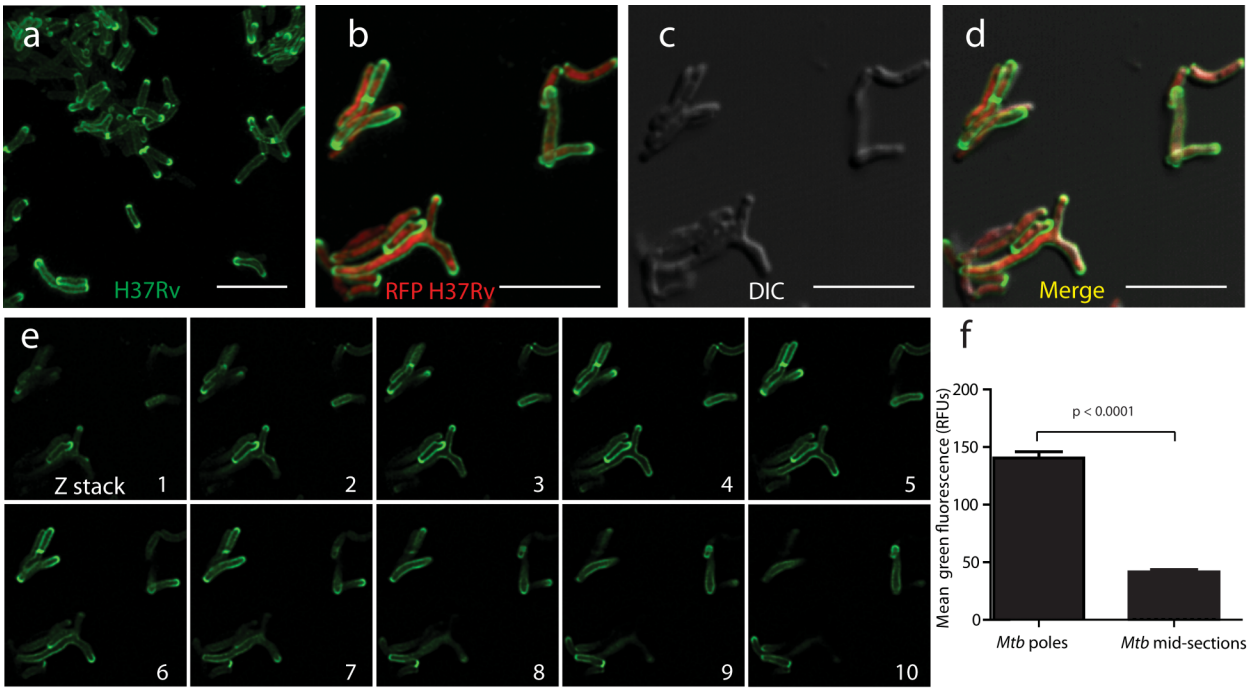

Figure 4. (a) H37Rv-*Mtb* are labeled with FITC-Tre and show signification accumulation of probe at the bacterial poles and membrane. (b) shows FITC-Tre labeling of the RFP (mCherry) expressing strain of H37Rv and (c) is the DIC image of (b), while (d) is an overlay of (b-c) and (e) depicts the Z stack (1-10) through the same image (step size of 0.13 µm) and demonstrates the FITC-Tre localization to the poles and membrane. (f) The mean fluorescence of poles and midsections of H37Rv Mtb, labeled with FITC-Tre, are quantified and show statistically significant differential labeling. RFUs = relative fluorescence units. Scale bars 5 µm.

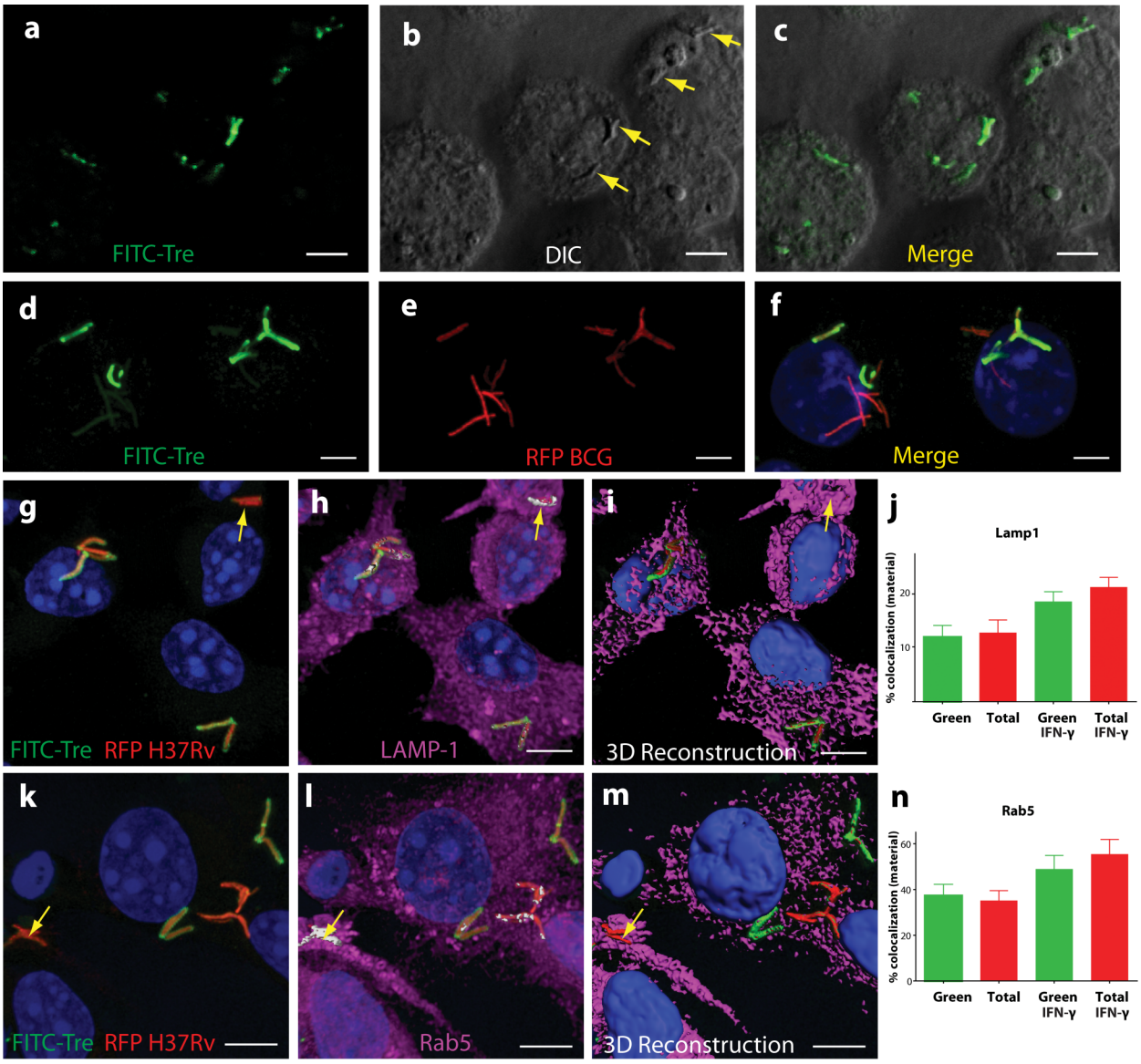

Figure 5. Heterogeneous labeling of individual bacilli within infected macrophages. Macrophages were infected with H37Rv-*Mtb* or *M. bovis* BCG expressing red fluorescent protein (RFP) where indicated. (a-c) J774 macrophages infected with H37Rv-*Mtb* and labeled with FITC-Tre. In the DIC image (b) the bacilli are indicated by yellow arrows. The merged image (c) shows good colocalization of FITC-Tre and *Mtb*. (d-f) depict J774 macrophages infected with BCG, expressing RFP (ds-red-1). (d) shows green labeling from FITC-Tre, (e) shows red labeling from RFP and (f) shows the merged images for (d) and (e). (g-i) illustrate

triple labeling colocalization studies with RFP, FITC-Tre and anti-LAMP-antibody in bone marrow macrophages (BMMs) activated with IFN-γ. Yellow arrows indicate red bacteria that are not green, ie do not take up FITC-Tre and that colocalize to a high degree with LAMP-1. (g) shows the merged RFP and FITC images, (h) shows the labeling with anti-LAMP-1 (magenta) with colocalization indicated in white, (i) shows a three dimensional reconstruction with all three labels superimposed. (j) shows the quantitation of this colocalization of LAMP-1 with bacteria that were labeled with FITC-Tre (green bars) or were red (total population). P-Values: Green vs. Total (ns), Green vs. Green+IFN-γ (0.006), Green vs. Total+IFN-γ (0.006), Total vs. Green + IFN-γ (0.01), Total vs Total+ IFN-γ (0.001) and Green+IFN-γ vs. Total+ IFN-γ (0.1). (k-m) depict colocalization studies with anti-Rab5 similarly infected and activated as in (g-i). Yellow arrows indicate red bacteria that are not green and that colocalize to a high degree with Rab5. (k) shows the merged RFP and FITC images, (l) shows the labeling with anti-Rab5-antibody (magenta) with colocalization indicated in white, (m) shows a three dimensional reconstruction with all three labels superimposed. (n) shows quantitation of colocalization of Rab5 with bacteria that were labeled with FITC-Tre (green bars) or were red (total population). P-Values: Green vs. Total (ns), Green vs. Green+IFN-γ (0.07), Green vs. Total+IFN-γ (0.02), Total vs. Green + IFN-γ (0.04), Total vs Total+ IFN-γ (0.008) and Green+IFN-γ vs. Total+ IFN-γ (ns). Error bars reflect standard error of the mean (SEM) for a minimum of three experiments. P value > 0.1 are notated not significant (ns). Scale bars 5 μm.